Monomeric chlorophyll *a enol*: Evidence for its possible role as the primary electron donor in photosystem I of plant photosynthesis

(ESR/redox potential/cation radical/electronic structure)

MICHAEL R. WASIELEWSKI, JAMES R. NORRIS, LESTER L. SHIPMAN, CHIH-PING LIN, AND WALTER A. SVEC

Chemistry Division, Argonne National Laboratory, Argonne, Illinois 60439

ABSTRACT The chlorophyll *a* (Chl *a*) special-pair model of the primary donor of photosystem I (P700) does not account in a completely adequate fashion for the magnetic resonance properties observed for P700$^+$. Moreover, P700 is at least 420 mV easier to oxidize than is Chl *a in vitro*. Neither Chl *a* dimer formation nor selective ligation of Chl *a* can account for this potential difference. Enolization of the Chl *a* ring V β-keto ester results in a very different π electronic structure. The Chl *a enol* can be trapped as a silyl *enol* ether. In addition, the *enol* analog 9-desoxo-9,10-dehydro-Chl *a* can be prepared. Both the trapped *enol* and its 9-H analog are $\approx$350 mV easier to oxidize than Chl *a*. The ESR spectrum of the cation radical consists of a single 6.1-G gaussian line that is line narrowed relative to that of Chl *a*$^+$ in a manner similar to P700$^+$. Electron-nuclear double resonance (ENDOR) spectroscopy resolves only a 3.5-MHz hyperfine splitting for the 3-methyl group. The remaining splittings are all less than 3.5 MHz. The second moment of the ESR line of fully ^{13}C-enriched 9-desoxo-9,10-dehydro-Chl *a*$^+$ agrees with that of [^{13}C]P700$^+$ to within 10%. Application of the special-pair model to the [^{13}C]P700$^+$ second-moment data yields a 100% error. *Ab initio* molecular orbital calculations on ethyl chlorophyllide *a enol* cation bear out the ESR and ENDOR data. We conclude that a monomeric Chl *a enol* model provides a better description of the magnetic resonance parameters and oxidation potential of P700 than a Chl *a* special-pair model.

Evidence concerning the structural nature of the primary photochemical electron donors of both bacterial and green plant photosynthesis is derived principally from ESR and electron-nuclear double resonance (ENDOR) spectroscopy of the oxidized donors. In purple photosynthetic bacteria such as *Rhodopseudomonas sphaeroides*, the oxidized primary donor P865$^+$ exhibits a single gaussian ESR signal having a linewidth that is narrowed by a factor of $1/\sqrt{2}$ relative to that of monomeric bacteriochlorophyll *a*$^+$ (BChl *a*$^+$) *in vitro* (1). The ENDOR spectrum of P865$^+$ shows that the hyperfine splittings of the oxidized donor are one-half those of monomeric BChl *a*$^+$ (2, 3). The assignment of the ENDOR signals to specific protons in BChl *a* is accomplished by selective biosynthetic deuteration of the chromophore. The hyperfine splittings of P865$^+$ can account for the total observed ESR linewidth of P865$^+$ only if the spin is shared equally between two BChl *a* molecules in P865$^+$.

Similar magnetic resonance studies of the photosystem I reaction center of green plants, P700, are much less definitive for several reasons. P700 reaction centers have not yet been obtained free from antenna chlorophyll *a* (Chl *a*). In addition, biosynthetic deuteration of selected protons of Chl *a* in algae has not been accomplished. Analysis of the ENDOR spectrum of P700$^+$ suggests that the methyl groups of the Chl *a* macrocycle in P700 may not be freely rotating at 77 K (2). This situation
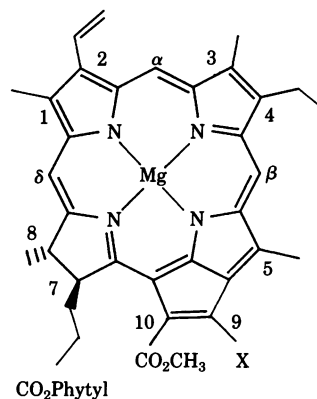
FIG. 1. Structure of Chl *a tert*-butyldimethylsilyl *enol* ether (X = *t*-BuMe$_2$Si) and of 9-desoxo-9,10-dehydro-Chl *a* (X = H).

complicates the interpretation of the P700$^+$ ENDOR results. Finally, P700$^+$ in algae grown with >90% ^{13}C enrichment yields an ESR signal whose lineshape is poorly fit by a spin-sharing dimeric model (4).

Another major difficulty in formulating a model for P700 involves its low oxidation potential. P700 is at least 420 mV easier to oxidize than is Chl *a in vitro* (5–8). This same situation does not prevail for P865 or for the primary donor of photosystem II, P680. P865 oxidizes only about 200 mV less positive than does BChl *a in vitro* (for review, see ref. 9), whereas P680 oxidizes 100–200 mV more positive than does Chl *a in vitro* (10). In previous studies of special-pair models, the oxidation potential of a given chlorophyll has never become less positive by more than $\approx$75 mV on covalent dimerization of the chlorophyll (11). Moreover, the work of Fajer and coworkers (12), independently confirmed in these laboratories (13), has shown that ligation of the central magnesium atom of Chl *a* with ligands of increasing nucleophilicity increases the oxidation potential of Chl *a* up to 200 mV. These results suggest that selective ligation of Chl *a* by the surrounding reaction center protein most likely cannot completely account for the dramatically low P700 oxidation potential.

This paper presents evidence that a reversible rearrangement of the geometric and π electronic structure of Chl *a* can account for the observed differences in redox and magnetic resonance properties between P700 and Chl *a in vitro*. The proposed rearrangement is the enolization of the ring V β-keto ester of Chl *a* (Fig. 1). The overall π electronic structure of the Chl *a enol* differs substantially from that of Chl *a* itself (see below).

Franck and Livingston originally suggested that the Chl *a enol* might have a role in green plant photosynthesis (14). They proposed that Chl *a* tautomerized following excitation. However, their notions found little or no experimental support. Sim-

Abbreviations: ENDOR, electron-nuclear double resonance; BChl *a*, bacteriochlorophyll *a*; Chl *a*, chlorophyll *a*; *t*-BuMe$_2$Si, *tert*-butyldimethylsilyl.

ilar ideas have been reexamined more recently (15), again with little experimental support. Our own work in this area has focused on trapping the Chl *a* enol and preparing Chl *a* derivatives possessing the same π system as the *enol* (16, 17). All of the previous theoretical and experimental studies have focused primarily on the optical properties of the *enol* with the result that the *enol* could not be assigned a function in the primary processes of green plant photosynthesis (18–21). The shift of the optical absorption band of Chl *a* from 663 to 700 nm constitutes only a 0.1-V change in energy, whereas the measured change in redox potential between monomeric Chl *a* and P700 approaches 0.5 V. Thus, the optical shift alone is a rather poor criterion for judging the applicability of a P700 model.

EXPERIMENTAL

Materials. Voltammetry and bulk electrolysis was performed in $CH_2Cl_2/0.1$ M (*n*-Bu)$_4$NClO$_4$. Purification of (*n*-Bu)$_4$NClO$_4$ and tetrahydrofuran has been described (13). Methylene chloride (Baker, HPLC grade) was dried twice for 24 hr over Linde 3A molecular sieves. The $CH_2Cl_2/0.1$ M (*n*-Bu)$_4$NClO$_4$ solution was treated with alumina for 24 hr prior to use (Woelm, activated at 450°C for 24 hr, 2 g of alumina/10 ml of solution). 9-Desoxo-9,10-dehydro-Chl *a* was prepared as described (16) except that magnesium insertion in the free ligand was accomplished by using Eschenmoser's procedure (22). Pheophytin *a* was obtained from the large-scale extraction of the blue-green alga *Spirulina maxima*. Chl *a* was prepared from pheophytin *a* as described (22). Chl *a* (99% ^{2}H) and Chl *a* (99% ^{2}H, 91% ^{13}C) were obtained from the corresponding isotopically labeled alga *Scenedesmus obliquus*, which was grown in our laboratory by using established procedures (23). The corresponding isotopically substituted 9-desoxo-9,10-dehydro-Chl *a* derivatives were prepared as above (16) except that sodium borodeuteride was used in the first reduction step. Both Chl *a* and 9-desoxo-9,10-dehydro-Chl *a* were purified by high-pressure liquid chromatography prior to use (Waters Associates, 30 cm $\times$ 7.8 mm inside diameter μ-Bondapak-C$_{18}$ column, elution with CH_3CN/15% tetrahydrofuran).

Preparation of Chl *a* *tert*-Butyldimethylsilyl enol Ether. All operations were carried out in a nitrogen-filled dry box. Chl *a* (90 mg, 0.1 mmol) was dissolved in dry dimethylformamide (20 ml). Dry pyridine (0.5 ml) was added, followed by *tert*-butyldimethylsilyl chloride (45 mg, 0.3 mmol). The resulting solution was stirred and bubbled with N_2 for 15 min. A solution of 2,6-di-*tert*-butyl-4-methylphenol (220 mg, 1.0 mmol) in CH_2Cl_2 (5 ml) was bubbled with dry N_2 for 5 min. *n*-Butyl-lithium (0.6 ml of a 1.6 M hexane solution, Aldrich) was added dropwise to the phenol solution. After 10 min, the lithium salt solution was added dropwise to the Chl *a* solution. The green Chl *a* solution rapidly turned yellow-green. After 30 min of stirring, the reaction mixture was poured into 0.25 M phosphate buffer (pH 7.0) and extracted with ether. The ether extract was washed four times with more buffer, dried over anhydrous Na_2SO_4, and evaporated. The crude product was chromatographed on Sepharose Cl-6B (24), eluting with 1.5% 2-propanol in hexane. The yellow-green product eluted, followed by unreacted Chl *a*. The yield of *enol* ether was 62 mg (62%).

Instrumentation. Cyclic and ac voltammetry were performed at a Pt-disc working electrode using Pt wire auxiliary and saturated calomel reference electrodes as described (13). Bulk electrolysis was carried out in a vacuum cell having a 5-ml capacity and using a Pt mesh basket working electrode with Pt wire auxiliary and pseudo reference electrodes. The cell was of conventional design equipped with a 1-mm-path-length optical cell. The electrochemical instrumentation has been described (13).

ESR spectra at both ambient and liquid helium temperatures were measured with a Varian E-9 system. ENDOR spectra were recorded with a custom-built instrument similar in design to that of Möbius (25). Optical absorption spectra were obtained with a Cary 14, and fluorescence emission spectra and quantum yields were determined with a custom-built fluorimeter (unpublished results). ^{1}H NMR spectra were obtained at 220 MHz using a Varian HR220 instrument in the pulse-Fourier transform mode.

RESULTS AND DISCUSSION

The *tert*-butyldimethylsilyl *enol* ether (26) of Chl *a* is more stable toward protonolysis than the corresponding trimethylsilyl derivative reported earlier (16). The increased stability allowed us to isolate the trapped *enol* and characterize it. In Table 1, the ^{1}H NMR chemical shifts of Chl *a* are compared with those of the trapped *enol* and of 9-desoxo-9,10-dehydro-Chl *a*. The resonances of the latter two compounds are shifted upfield relative to those of Chl *a*. The largest relative shifts are $\approx$2 ppm for the methine protons. Significantly, the proton chemical shifts of the trapped *enol* are virtually identical to those of the 9-desoxo compound. It is well known that Chl *a* possesses a diamagnetic ring current that shifts the resonances of protons near the macrocyclic plane to unusually low field (27). The insertion of a 9,10 double bond into the π system of the macrocycle significantly perturbs its electronic structure. This perturbation results in a diminution of the ring current that is similar for both the silyl *enol* ether and the 9-desoxo compound. A similar effect has been observed in the ^{1}H NMR spectra of the magnesium *enolate* of methyl pheophorbide *a* (21) and Eschenmoser's cyclochlorophyllide *a enols* (19, 20).

The perturbation of the Chl *a* π electronic system by a 9,10 double bond further manifests itself in the electronic spectra of these derivatives. Fig. 2 compares the spectrum of Chl *a* with those of the trapped *enol* and 9-desoxo-9,10-dehydro-Chl *a* in acetone. The spectra are characterized principally by a decrease in the extinction coefficient of the principal red band and a splitting of the Soret band relative to that of Chl *a*.

Table 1. Proton chemical shifts

	δ, ppm		
Proton	Chl *a*	Chl *a* t-BuMe$_2$Si *enol* ether	9-Desoxo-9,10-dehydro-Chl *a*
β-H	9.56	7.94	7.94
α-H	9.36	7.86	7.76
2a-H	8.08	7.46	7.44
δ-H	8.28	6.86	6.81
9-H	—	—	6.67
10-H	6.11	—	—
2b-H$_A$	6.15	5.82	5.81
2b-H$_B$	6.06	5.75	5.72
7-H	4.06	4.19	4.28
10b-CH$_3$	3.89	3.78	3.80
8-H	4.40	4.44	4.47
4a-CH$_2$	3.81	3.17	3.15
5-CH$_3$	3.72	2.75	2.67
3-CH$_3$	3.36	2.75	2.72
1-CH$_3$	3.33	2.79	2.78
4b-CH$_3$	1.76	1.50	1.42
8a-CH$_3$	1.60	*	*

NMR spectra were recorded at 20°C in 1% [^{2}H$_5$]pyridine in CCl$_4$ at 5 mM. The assignments of the proton resonances of the 9-desoxo compound are based on preliminary differential line broadening data (E. Sitzmann, private communication) of the signals in the presence of tris(*p*-bromophenyl)ammonium hexachloroantimonate. The assignments of the proton resonances of the *enol* ether are by analogy to the 9-desoxo compound. These assignments should be regarded as tentative.
* The 8a-CH$_3$ group resonance is hidden by the phytyl multiplet at 0.8–1.6 δ.
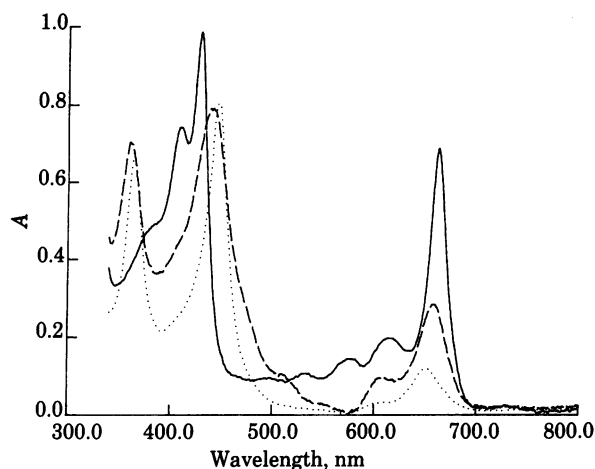
FIG. 2. Electronic absorption spectra of 8 μM solutions of Chl *a* (——), Chl *a tert*-butyldimethylsilyl *enol* ether (– – –), and 9-desoxo-9,10-dehydro-Chl *a* (···) in acetone.

The trapped *enol* and 9-desoxo-9,10-dehydro-Chl *a* have fluorescence quantum yields of <0.005 and apparent fluorescence emission maxima at 662 nm and 651 nm, respectively. Under the same conditions Chl *a* fluoresces with a 0.35 quantum yield. Because these fluorescence yields are very low, they cannot be assigned with complete confidence to the *enolic* derivatives. The loss of the fluorescence decay channel in these molecules may relate in a biomimetic sense to the very low or nonexistent fluorescence yield of P700 (28). Yet, the photophysical reasons behind these two observations may be different. An attempt to observe the photoexcited triplet state of 9-desoxo-9,10-dehydro-Chl *a* at 8 K by ESR has not been successful. Under our experimental conditions, this result suggests that either the triplet has a lifetime that is significantly less than 100 μsec or the triplet yield is very small (or both).

The oxidation potentials for the Chl *a* trapped *enol* and 9-desoxo-9,10-dehydro-Chl *a* are compared with those of Chl *a* and P700 in Table 2. The key observation is the dramatic decrease of the oxidation potential of Chl *a* on insertion of a 9,10 double bond. The presence of the oxygen atom at position 9 in the trapped *enol* is a minor perturbation on this effect, contributing only an additional 50 mV to the total oxidation potential change. The oxidation potentials of both the trapped *enol* and the 9-desoxo derivative approach that of P700. The remaining potential difference is well within the range that ligation or protein environment effects could be expected to contribute. The oxidations are reversible in the absence of hydroxylic solvents.

Coulometry during bulk electrolysis of the 9-desoxo compound confirms that one electron per molecule is removed at potentials slightly more positive than $E_{1/2}$ for the first oxidation wave. Preliminary data suggest that the optical absorption spectrum of 9-desoxo-9,10-dehydro-Chl *a*$^+$ is similar to that of Chl *a*$^+$ with an absorption at 800 nm.

Table 2. Oxidation potentials

Substance	$E_{1/2}^+$, mV	$E_{1/2}^{2+}$, mV
Chl *a*	860	1100
9-Desoxo-9,10-dehydro-Chl *a*	550	890
Chl *a*-tBuMe$_2$Si *enol* ether	500	850
P700	370–520*	—

Potentials were recorded by using a saturated calomel reference electrode but are listed in reference to the normal hydrogen reference electrode.
* Refs. 5–8. The potential depends primarily on whether whole chloroplasts or P700-enriched subchloroplast preparations are used.

ESR spectra of 9-desoxo-9,10-dehydro-Chl *a*$^+$ were recorded on 0.1 mM solutions of cation in CH$_2$Cl$_2$/0.1 M (*n*-Bu)$_4$NClO$_4$. The microwave power and 100-kHz modulation amplitude were maintained at levels sufficiently low to prevent saturation and artificial broadening of the signals. ESR linewidths and their second moments (29) are given in Table 3 for Chl *a*$^+$, 9-desoxo-9,10-dehydro-Chl *a*$^+$, P700$^+$, and several of their isotopically substituted species.

The ESR linewidth of 9-desoxo-9,10-dehydro-Chl *a*$^+$ is narrowed relative to that of Chl *a*$^+$ and is only 0.9 G narrower than that of P700$^+$. Thus, the spin distribution of monomeric 9-desoxo-9,10-dehydro-Chl *a*$^+$ must differ substantially from that of Chl *a*$^+$. Yet, the ESR signal of the 9-desoxo compound is approximately gaussian, which implies that the carbon atoms α to the methyl groups, the carbon atoms α to protons, and the central nitrogen atoms do not possess large spin density. Similar comments apply to the fully deuterated 9-desoxo derivative. The roughly sixfold decrease in the magnetic moment of deuterons relative to protons results in a substantially narrower ESR line. Yet, the ESR linewidth ratio $(\Delta H)_{1H}/(\Delta H)_{2H}$ for 9-desoxo-9,10-dehydro-Chl *a*$^+$ is 1.9 while the same ratio for monomeric Chl *a*$^+$ is 2.4. This fact, together with the gaussian lineshape, suggests that a larger fraction of the second moment of the 9,10-dehydro cation ESR line is determined by contributions other than proton hyperfine interactions (29).

The ESR lineshape of ^{13}C-enriched 9-desoxo-9,10-dehydro-Chl *a*$^+$ is nongaussian, as are those of ^{13}C-enriched P700$^+$ and Chl *a*$^+$. The peak-to-peak linewidth of the ^{13}C-enriched 9-desoxo cation equals that of P700$^+$ to within experimental error. More important, the second moment of the ESR line of the ^{13}C-enriched 9-desoxo cation agrees with that of P700$^+$ to within 10%. The second-moment criterion is an especially sensitive indicator of the actual number of nuclei contributing to the total ESR linewidth. Given the standard assumption that the ^{13}C hyperfine splittings are linear functions of the spin densities at carbon, the special-pair model demands that the second moment of the P700$^+$ ESR line be one-half that of monomeric Chl *a*$^+$. The data in Table 2 show that this is not the case. This fact suggests that the redistribution of spin density characteristic of P700$^+$ may be an intramolecular consequence of the presence of a hypothetical oxidized monomeric Chl *a* enol rather than an intermolecular result of spin sharing between two Chl *a* macrocycles from which one electron has been removed.

Table 3. ESR data

Substance	ΔH_{pp}, G	$\langle \omega^2 \rangle$ G^2
Chl *a*$^+$	9.3	21.6*
[^{2}H]Chl *a*$^+$	3.8	3.6*
[^{2}H,^{13}C]Chl *a*$^+$	11.5	85.0†
(Chl *a*)$_2^+$‡	6.6	10.8
([^{2}H]Chl *a*)$_2^+$‡	2.7	1.8
([^{2}H,^{13}C]Chl *a*)$_2^+$‡	8.1	42.5
9-Desoxo-9,10-dehydro-Chl *a*$^+$	6.1	9.3*
9-[^{2}H]Desoxo-9,10-dehydro-Chl *a*$^+$	3.2	2.6*
9-[^{2}H,^{13}C]Desoxo-9,10-dehydro-Chl *a*$^+$	13.2	96.0†
P700$^+$	7.1	12.6*
[^{2}H]P700$^+$	3.0	2.3*
[^{2}H,^{13}C]P700$^+$	12.0	86.6†

All radicals *in vitro* are 0.1 μM solutions in CH$_2$Cl$_2$/0.1 M (*n*-Bu)$_4$NClO$_4$; *g* = 2.0025 ± 0.002. All spectra were obtained at 8 K.
* Based on a gaussian lineshape where $\langle \omega^2 \rangle = \Delta H_{pp}^2/4$.
† Determined by computer analysis of the entire nongaussian lineshape. Uncertainties of ±15% may be expected.
‡ Calculated: linewidths are $1/\sqrt{2}\ \Delta H_{pp}$ for the monomers, and second moments are one-half those of the monomers.
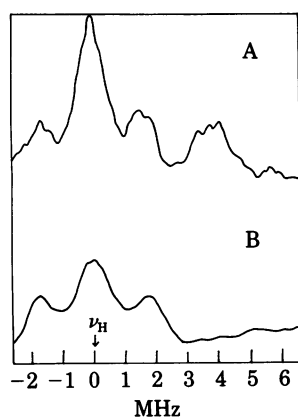
FIG. 3. ENDOR spectra of 1 mM Chl a^+ (A) and 1 mM 9-desoxo-9,10-dehydro-Chl a^+ (B) at 77 K. The cations were generated electrochemically in CH_2Cl_2/0.1 M (n-Bu)$_4$NClO$_4$ containing 5% tetrahydrofuran.

To investigate this point further, we obtained an ENDOR spectrum of 9-desoxo-9,10-dehydro-Chl a^+ at 77 K. This spectrum and that of Chl a^+ obtained under the same conditions are shown in Fig. 3. It is obvious that 9-desoxo-9,10-dehydro-Chl a^+ possesses no large β-proton hyperfine splittings. This result is consistent with its ESR linewidth. Also, the central portion of the spectrum surrounding the free proton frequency is broad. A central broadening of the ENDOR spectrum has been observed for P700$^+$ but significantly not for P865$^+$. This broadening may be due to an increase in the protic environment of P700 or the presence of many small hyperfine splittings. The spectrum of the 9-desoxo cation suggests that the broad center region may be due to the latter reason.

The large 11.8-MHz and 7.5-MHz splittings in the ENDOR spectrum of Chl a^+ have been assigned to the 7,8 protons and the 5-methyl group, respectively (30). The largest coupling clearly visible in the 9-desoxo cation spectrum is 3.5 MHz. Apart from the central broad region, two low-intensity transitions are clearly visible at 3.7 and 5.4 MHz in the P700$^+$ ENDOR spectrum (2). The weak intensity of these signals has been presented as evidence that the methyl groups of P700 *in vivo* may be undergoing hindered rotation. The ENDOR spectrum of P700$^+$ is difficult to interpret in a straightforward fashion

and its definitive analysis will await selective isotopic labeling of P700. Yet, if one assumes that hindered rotation occurs, it can be easily shown that the ENDOR spectrum of the 9-desoxo cation is consistent with that of P700$^+$.

The β-proton hyperfine splitting a is related to a constant B, the π spin density at the adjacent unsaturated carbon atom ρ_c^π, and the dihedral angle (θ) between the π orbital of the carbon adjacent to the β proton and the C_α—H bond by Eq. 1 (31)

$$a \cong \rho_c^\pi B \cos^2\theta. \qquad [1]$$

As the methyl group responsible for the 3.5-MHz coupling of the 9-desoxo cation is freely rotating, $\langle\cos^2\theta\rangle = \frac{1}{2}$. Thus, $\rho_c^\pi B = 7.0$ MHz. If this methyl group undergoes restricted rotation, hyperfine splittings at 0–7 MHz are possible. As the P700$^+$ ENDOR spectrum shows hyperfine splittings less than 7 MHz, the ENDOR data for P700$^+$ are consistent with the ENDOR data for monomeric 9-desoxo-9,10-dehydro-Chl a^+. The P700$^+$ ENDOR data can also be made to fit the special pair model, but the P700$^+$ second-moment data cannot be fit to the correct number of nuclei required by the special pair model. Thus, although the ENDOR evidence considered alone cannot distinguish between the two models, the magnetic resonance data taken as a whole favors the oxidized Chl a enol model of P700$^+$.

To explain the ESR and ENDOR data an *ab initio* self-consistent field calculation was performed on the ethyl chlorophyllide a enol using the structure depicted in Fig. 4. The methodology and basis set used were similar to those used in a study of ethyl chlorophyllide a (32). The π spin densities correspond to the electron distribution in the highest occupied molecular orbital of the closed shell neutral molecule. The π spin densities for the cation radical are given in Fig. 4. Several features of the spin distribution should be pointed out. First, virtually no spin density is found on carbons 2, 5, 7, and 8, whereas carbons 1, 3, and 4 bear spin densities similar to those calculated for Chl a^+. Second, the spin distribution is very asymmetric: four carbon atoms associated with rings II, III, and V that are not bonded to either methyl groups or protons bear ≈53% of the total spin density. Third, only small spin densities are found on the 9-carbon atom and its associated oxygen atom.
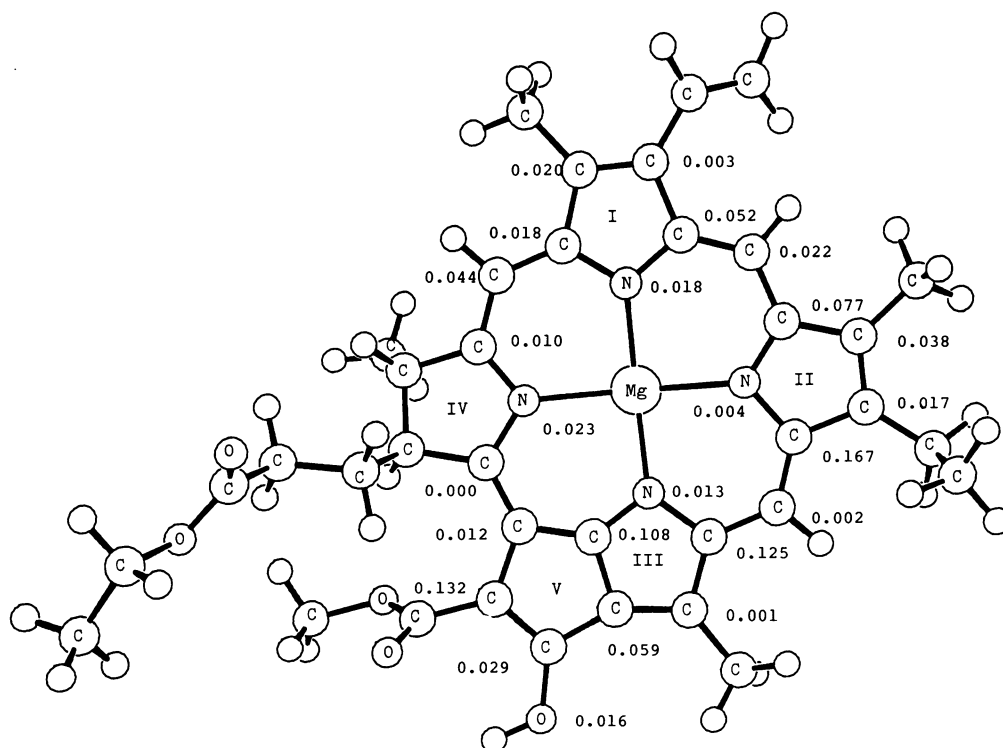
FIG. 4. Calculated π spin densities for the ethyl chlorophyllide a enol cation radical.

As the calculations predict that only $\approx 1.6\%$ of the spin in the *enol* cation is localized on the 9-oxygen atom, the ESR and ENDOR properties of 9-desoxo-9,10-dehydro-Chl a^+ should be similar to those of the *enol* cation. As four carbon atoms that are more than two bonds removed from protons bear 53% of the spin density, the ESR linewidths of both the protonated and deuterated species are expected to remain small relative to Chl a^+. Moreover, the highest spin densities are distributed over four carbon atoms, so that no individual ^{13}C splitting is large enough to be resolved. Yet, the spin densities are high enough to result in a nongaussian lineshape.

The ENDOR spectrum of 9-desoxo-9,10-dehydro-Chl a^+ agrees with the calculated trends in the spin density distribution. As the largest calculated spin density on a carbon atom adjacent to a methyl group occurs at position 3, the 3.5-MHz splitting (see Fig. 3) is assigned to the 3-methyl group. The predominance of small hyperfine splittings is consistent with the analysis of the P700$^+$ ENDOR spectrum presented above.

CONCLUSIONS

We regard the Chl *a enol* model as a working hypothesis subject to further refinement. For example, the data obtained thus far cannot answer two important questions. First, does P700 exist as a monomeric *enol* in the dark or is the *enol* a transient photochemical intermediate preceding photooxidation of P700? Second, if the *enol* exists in the dark, does it bind to the reaction center protein as an *enol, enolate* ion, or covalent *enol* ester? *keto-enol* tautomerism is an equilibrium process, and extraction of the hypothetical *enol* from the protein would result in isomerization back to *Chl a.*

It is important to reiterate that our magnetic resonance data probe only the final oxidized state of P700 and the *enol* derivatives. The redox potentials provide additional information about the nature of the transition state for oxidation of P700 and the *enol* derivatives. The redox data suggest that the *enol*ic character of the donor must be reflected in the transition state for oxidation. Our data, taken as a whole, suggest that an oxidized Chl *a enol* model provides a more satisfying alternative description of P700$^+$ than does the Chl *a* special pair model. No additional conclusions about the relationship of the *enol* to P700 can be made based on the data presented here.

Thus, working within this expanded conceptual framework, further critical tests of these models and additional work on P700 will better define the nature of the primary electron donor of photosystem I.

1. Norris, J. R., Uphaus, R. A., Crespi, H. L. & Katz, J. J. (1971) *Proc. Natl. Acad. Sci. USA* **68,** 625–628.
2. Norris, J. R., Scheer, H., Druyan, M. E. & Katz, J. J. (1974) *Proc. Natl. Acad. Sci. USA* **71,** 4897–4900.
3. Feher, G., Hoff, A. J., Isaacson, R. A. & McElroy, J. D. (1975) *Ann. N.Y. Acad. Sci.* **244,** 239–259.
4. Norris, J. R., Uphaus, R. A. & Katz, J. J. (1972) *Biochim. Biophys. Acta* **275,** 161–168.
5. Kok, B. (1961) *Biochim. Biophys. Acta* **48,** 527–532.
6. Knaff, O. B. & Malkin, R. (1973) *Arch. Biochem. Biophys.* **159,** 555–562.
7. Evans, M. C. W., Sihra, C. K. & Slibus, A. R. (1977) *Biochem. J.* **162,** 75–85.
8. McIntosh, A. R., Manikowski, H. & Bolton, J. R. (1979) *J. Phys. Chem.* **83,** 3309–3313.
9. Prince, R. C. & Dutton, P. L. (1978) in *The Photosynthetic Bacteria,* eds. Clayton, R. C. & Sistrom, W. R. (Plenum, New York), pp. 439–453.
10. Bearden, A. J. & Malkin, R. (1975) *Q. Rev. Biophys.* **7,** 131–177.
11. Wasielewski, M. R. (1978) in *Frontiers of Biological Energetics,* eds. Dutton, P. L., Leigh, J. S. & Scarpa, A. (Academic, New York), Vol. 1, pp. 63–72.
12. Davis, M. S., Forman, A. & Fajer, J. (1979) *Proc. Natl. Acad. Sci. USA* **76,** 4170–4174.
13. Wasielewski, M. R., Smith, R. L. & Kostka, A. G. (1980) *J. Am. Chem. Soc.* **102,** 6923–6928.
14. Franck, J. & Livingston, R. (1941) *J. Chem. Phys.* **9,** 184–190.
15. Fetterman, L. M., Galloway, L., Winograd, N. & Fong, F. K. (1977) *J. Am. Chem. Soc.* **99,** 653–655.
16. Wasielewski, M. R. & Thompson, J. F. (1978) *Tetrahedron Lett.,* 1043–1046
17. Hynninen, P. H., Wasielewski, M. R. & Katz, J. J. (1979) *Acta Chem. Scand. Ser. B* **33,** 637–648.
18. Song, P. S., Moore, T. A. & Sun, M. (1972) in *The Chemistry of Plant Pigments,* ed. Chichester, O. (Academic, New York), pp. 44–45.
19. Falk, H., Hoornaert, G., Isenring, H.-P. & Eschenmoser, A. (1975) *Helv. Chim. Acta* **58,** 2347–2357.
20. Isenring, H.-P., Zass, E., Smith, K., Falk, H., Luisier, J.-L. & Eschenmoser, A. (1975) *Helv. Chim. Acta* **58,** 2357–2367.
21. Sheer, H. & Katz, J. J. (1978) *J. Am. Chem. Soc.* **100,** 561–571.
22. Zass, E., Isenring, H.-P., Etter, R. & Eschenmoser, A. (1980) *Helv. Chim. Acta* **63,** 1048–1067.
23. Taecker, R. G., Crespi, H. L., DaBoll, H. F. & Katz, J. J. (1971) *Biotechnol. Bioeng.* **13,** 779–793.
24. Omata, T. & Murata, N. (1980) *Photochem. Photobiol.* **31,** 183–185.
25. Dinse, K.-P., Möbius, K. & Biehl, R. (1973) *Z. Naturforsch. A* **28,** 1069–1080.
26. Corey, E. J. & Venkateswarlu, A. (1972) *J. Am. Chem. Soc.* **94,** 6190–6191.
27. Sheer, H. & Katz, J. J. (1975) in *Porphyrins and Metalloporphyrins,* ed. Smith, K. (Elsevier, Amsterdam), pp. 399–524.
28. Lavorel, J. & Etienne, A.-L. (1977) in *Primary Processes of Photosynthesis; Topics in Photosynthesis,* ed. Barber, J. (Elsevier, Amsterdam), Vol. 2, pp. 205–268.
29. Vincow, G. & Johnson, P. M. (1963) *J. Chem. Phys.* **39,** 1143–1153.
30. Scheer, H., Katz, J. J. & Norris, J. R. (1977) *J. Am. Chem. Soc.* **99,** 1372–1381.
31. Heller, C. & McConnell, H. (1960) *J. Chem. Phys.* **32,** 1535–1539.
32. Petke, J. D., Maggiora, G. M., Shipman, L. L. & Christoffersen, R. E. (1980) *Photochem. Photobiol.* **31,** 243–257.